analytical chemistry

Article

pubs.acs.org/ac

High-Resolution Mobility Analysis of Charge-Reduced Electrosprayed Protein Ions

Juan Fernandez de la Mora*

Department of Mechanical Engineering-Materials Science, Yale University, New Haven, Connecticut 06520, United States

Supporting Information

ABSTRACT: Many mobility studies (IMS) of electrospray ions with charge states z reduced to unity have shown a singular ability to analyze large protein complexes and viruses, though with wide mobility peaks (fwhm ~ 20%). Here we confirm that this limitation arises primarily when *early charge reduction* precedes drop evaporation (suppressing secondary atomization by the usual sequence of many Coulomb explosions). By drying before neutralizing, we achieve a protein fwhm of ~3.7%. A positively biased electrospraying capillary is coaxial with a cylindrical charge-reduction (CR) chamber coated with radioactive Ni-63 (10 mCi) that fills the CR chamber with a bipolar ionic atmosphere. A screen interposed between the spraying capillary and the CR chamber limits penetration of the neutralizing anions into the electrospray (ES) chamber, precluding destabilization of the ES tip, even when brought ~~arbitrarily~~ close to the grid to enhance ion transmission. As ES cations cross the grid, driven by their own space charge, they recombine with CR ions reducing their charge state as well as space charge dispersion. The setup is tested with the protein ovalbumin (M_W ~ 44.3 kDa) and its clusters up to the tetramer, by analyzing the charge-reduced ions with a differential mobility analyzer (DMA). At gas sample flow rates of ~1 L/min, the dominant peaks are singly charged (z = 1). They are widened by clustering of involatile solution impurities, depending on spray quality and solution cleanness, with fwhm as small as 3.7% achieved in desalted and acidified solutions. When using sharp nanospray capillaries, the grid may be removed, resulting in ~2-fold increased ion transmission. In the absence of the grid, however, spray stability and quality are often compromised, even with capillary tip diameters as small as 30 μm.

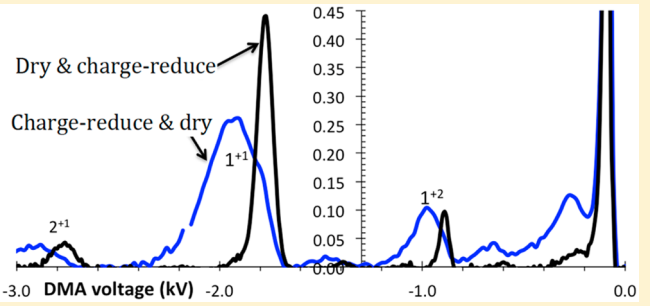

Electrospray ionization (ESI) converts involatile solutes into gas phase ions for mass spectrometry (MS)[1] or for alternative gas phase analyses such as ion mobility spectrometry (IMS). ESI's tendency to form multiply charged ions is advantageous to widen the mass spectrometer's mass range. However, it greatly increases the number of peaks present, often resulting in unresolvable spectral complexity.[2] For this reason, various charge-reduction techniques have been proposed,[3−5] with maximal spectral simplification achievable by producing dominantly singly charged ions. This drastic level of charge reduction is incompatible with the limited mass range of MS detectors in studies of large protein complexes and viruses. However, IMS permits the analysis of singly charged ions of considerable sizes: Certainly up to 30 nm with resolving powers approaching (and possibly exceeding) 40[6] and even larger sizes with some resolution concessions.[7] Furthermore, such massive ions can be detected individually at ambient conditions by growing them into visible drops via vapor condensation in so-called condensation nucleus counters, CNCs (also called condensation particle counters, CPCs).[5] This sensitive detector is not easily coupled to conventional drift time IMS systems due to its relatively slow response time (~1 s). However, new IMS designs with response times >1 s have already shown promise in the protein size range,[8] and when combined with faster CNCs,[9] will surely improve their current resolving power approaching 20. Differential mobility analyzers (DMAs) have long been compatible with slow detectors,[10] whence their combination with charge-reduced electrospray and a CNC detector, termed GEMMA,[5] has demonstrated considerable advantages for the analysis of large biological ions much harder to study by mass spectrometry.[11−14]

The main shortcoming of GEMMA is its limited mobility resolution, typically fwhm >20% for proteins (i.e., Figure 4a of ref 7). In contrast IMS spectra of electrosprayed proteins give fwhm ~3−4%, both in conventional drift time IMS and in studies based on high-resolution DMAs, including cases with charge reduction (Figure 2 of ref 15). This fact, together with the ability of DMAs to reach resolving powers as high as 100,[16] suggests that an improved GEMMA-like method should enable good ion transmission and a resolving power of ~30, limited only by the natural coexistence of several gas phase protein conformations. We have previously reasoned that the limited resolution of GEMMA results from its unconventional electrospraying method (connected to the charge reduction

Received: November 10, 2014
Accepted: March 13, 2015

DOI: 10.1021/ac504445n
Anal. Chem. XXXX, XXX, XXX−XXX

step), giving rise to a substantial and variable level of clustering of involatile residue material on the protein ion.[15,17,18] However, the alternative ES-charge-reduction approaches we have proposed have not been adopted by other groups, perhaps because our charge reduction efficiency, transmission, and peak width have not been sufficiently optimized or documented. However, recent signs of increased interest in higher resolution variants of GEMMA must be noted. A first combination of GEMMA's charge reduction with several DMAs reported clearly more compact protein structures for the DMA having a higher resolving power.[19] A more recent investigation with another DMA of even higher resolving power[6] found also modest peak width reductions with some native proteins: fwhm > 17.6% for all but one (14.7% for ovalbumin).[14] However, a drastic peak narrowing was discovered for several small and strongly denatured proteins, with fwhm as low as 8.5%.[14] Good DMA resolution is hence necessary but not sufficient to achieve narrow peaks.

The acidification advantage observed[14] is of great intrinsic interest, offering superficial analogies with the well-known (but not so well understood) role of acids in reducing clustering in ES-MS (and ES-IMS[14]). A linear chain (including denatured proteins) can apparently be extruded cleanly out of the drop,[20,21] whereas globular proteins remain imprisoned in the drop until it dries, inheriting its full load of involatile material.[22] Unfortunately, protein extrusion is unlikely to happen in singly or doubly charged drops, so the peak narrowing observed in ref 14 calls for a different explanation. Acidification is in any case not a general antidote against an imperfect electrospray, first because it is not viable in the case of protein complexes falling apart at unnatural pH, and also because the observed beneficial effect is minimal at protein masses beyond 40 kDa (fwhm = 14.7% → 13.4% for ovalbumin).[14] Another notable exception to GEMMA's generally wide peaks has been recently reported for viruses, with fwhm in some cases below 5%.[23] This exceptional narrowness probably follows from the closer match between the diameters of the virus and the initial ES drop, which results in a relatively small level of adduction. In conclusion, it appears that much of the resolution problem noted in the case of proteins results from the unusual ESI conditions used in GEMMA. The ES-charge reduction process will therefore be the focus of the present attempt at augmenting the performance of the method.

■ ATMOSPHERIC PRESSURE CHARGE-REDUCTION CHAMBER DESIGN

The key to minimize spectral complexity is to reduce the charge state to unity ($z = 1$), perhaps tolerating a small contribution of doubly charged ions ($z = 2$). Here we shall discuss only charge-reduction methods involving the interaction of the ES ions with a bipolar mixture of singly charged anions and cations, produced by ionizing radiation (radioactive sources, UV, X-rays) in an initially neutral gas at near ambient pressure. For multiply charged cations, the initial z evolves by interacting with monovalent anions, going sequentially through all the lower charge states $z \rightarrow z - 1 \rightarrow z - 2, ..., \rightarrow 1$. If insufficient reaction time is given, multiply charged ions survive. For an excessive time, even singly charged ions are neutralized, leading to poor conversion into the $z = 1$ product sought. An optimal reaction time t^* may therefore be chosen to maximize the magnitude of the $z = 1$ peak such that the probability of surviving $z = 2$ ions is below a desired threshold.[15] Unfortunately this optimal time depends weakly on the initial charge states z_{in} as $t^*(z_{in}) \sim \ln(z_{in})$,[15] biasing slightly the signal intensity and complicating quantification in complex mixtures. This difficulty has been ingeniously circumvented in the GEMMA design by tuning t^* for the initial ES drops (before they undergo a first Coulomb explosion), which may be produced with relatively good uniformity of size and charge.[24] The drawback of this *early neutralization* is that the volume of involatile residue that adducts to the final protein ions is that contained in the volume of the original ES drop, rather than that in the much smaller final drops produced by the usual long series of Coulomb explosions. This increased adduction decreases artificially the mobility and widens the peak in a fashion reflecting the width of the size distribution of the original ES drops. Accordingly, *early neutralization* is not ideal for resolution.

Early neutralization is not optimal either for sensitivity. Indeed, ES drops may be initially 10 nm in diameter and may complete evaporation in submicrosecond times. Accordingly, achieving drop neutralization prior to the first Coulomb explosion requires special measures, such as a relatively high humidity in the ES chamber[25] and initial drops larger than those achievable in ES practice. For instance, Kaufman and colleagues use 20 mM aqueous ammonium acetate,[5,7] while 100 mM (manageable in practice) would produce typical initial drop volumes 5 times smaller.[26] The larger initial drop diameters and humidities used to delay drop evaporation also delay the production of analyte ions, resulting in higher space charge broadening and dilution of the ion cloud. Furthermore, the solution concentration must be tuned such that each final drop contains at most one analyte ion, forcing much smaller solution concentrations in initially large nonexploding drops than with initially small drops further atomized by Coulombic explosions. Therefore, both from the sensitivity and the resolution point of view, it is better to produce the smallest possible ES drops and evaporate them as completely and as swiftly as possible, as amply confirmed by the nanospray experience. Space charge dilution of the ion cloud evidently continues after complete drop drying, whence fast sampling into an analytical instrument is usually desirable. In our case, the ions must first be charge-reduced, which decreases drastically the space charge field E as well as the analyte ion mobility Z (hence the space charge dilution velocity ZE). Accordingly, one should inject the analyte ions into the charge-reduction chamber immediately following complete drop drying but not before. There is however a difficulty. The formation of a Taylor cone takes place ordinarily at the interface between a conducting fluid (the solution) and an insulating medium (the surrounding gas). If the electric field from the capillary tip penetrates into the charge-reduction region, some of the free ions present there are drawn into the electrospraying chamber and the medium surrounding the Taylor cone ceases to be insulating. Little is known on the physics of Taylor cone formation under such conditions, other than the readily observable fact that the range of stability of the electrospray is severely curtailed, very much as in situations where an electrical discharge forms at the liquid tip.

Note finally that analyte quantification (relating the measured gas phase concentration to the original solution concentration) when *drying before neutralizing* is in principle as viable as when *neutralizing before drying*. Both require corrections due to the size dependence of transport losses and charge-reduction efficiency (both losses are also charge-dependent, but only size counts since the charge on large

DOI: 10.1021/ac504445n
Anal. Chem. XXXX, XXX, XXX−XXX

biomolecules scales approximately with the 1/2 power of molecular volume[22]).

Charge-Reduction Chamber. A simple ES charge-reduction design addressing the various points just discussed is shown in Figure 1. The ES chamber (left, with window) is

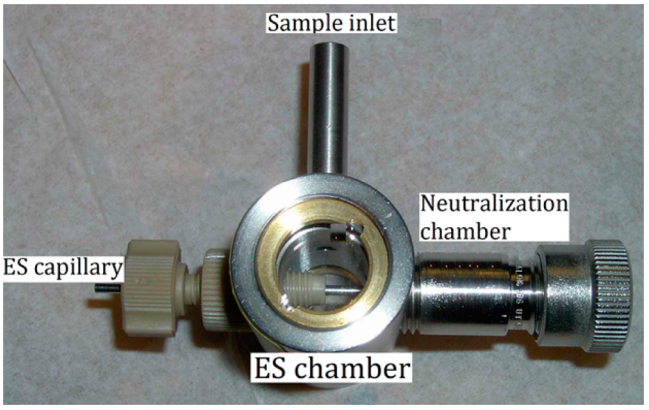

Figure 1. Electrospray chamber (center left) with frontal window. A spraying capillary enters from the left, coaxially with the charge-reduction chamber (right). Gas enters from the top tube, conveying charged particles into the charge-reduction chamber.

separated from the cylindrical charge-reduction (CR) chamber (Cajon fitting, screwed to right of the ES chamber) by a thin plate orifice 5 mm in diameter. The capillary emitter is introduced through the left via a tight fitting (gray), coaxially with this orifice and with the CR chamber, so that the emitter tip can be moved up and down the axis, including positions upstream and downstream the thin plate. The inner diameter of the CR chamber is slightly larger than the outer diameter of the radioactive source, a thin walled Ni cylinder 0.775 cm in outer diameter, 0.7 cm in length (Eckert and Ziegler). The wall of this source is coated with 10 mCi of radioactive Ni-63 (~101 years half-life), producing β particles with a maximal energy of 67 keV. The rate of ion pair generation within the small volume inside the Ni cylinder can be inferred from the maximal current of 2.2 nA received when replacing the capillary by a metallic cylinder 1/16 in. in diameter (shown in Figure 1), electrically biased with respect to the Ni cylinder in CO_2 gas at room temperature and pressure. In order to control the undesirable penetration of neutralizing ions into the ES chamber, in addition to varying the axial position of the capillary tip, various washers and screens could be placed immediately downstream the 5 mm thin plate orifice. The charge-reduction chamber is slightly longer than twice the length of the Ni source, whence additional control could be achieved by putting the source either immediately downstream the thin plate orifice or 0.7 cm downstream from it. The first (closer) position was mainly investigated here, though several experiments used two 10 mCi sources in series.

EXPERIMENTAL SECTION

A flow rate typically of 1 or 2 L/min of bottled dry air or CO_2 entered through the top tube (Figure 1) into the ES chamber, conveyed the electrosprayed protein ions through the thin plate orifice separating the ES chamber from the CR chamber, and carried them through the CR chamber into the inlet of a differential mobility analyzer of the Half-Mini type,[6] where their mobility was determined. Mobility spectra are obtained by fixing an axial flow of drift gas in the DMA, a sample inlet and outlet flow rates, and scanning over the voltage difference between the two cylindrical electrodes containing an inlet and an outlet slit, respectively. Under these conditions the DMA voltage is strictly proportional to the inverse ion mobility, through a calibration constant determined here with the mobility standard $(C_{18}H_{37})_4N^+$ (C18), the most mobile peak produced by electrospraying an ethanol solution of tetraoctadecylammonium bromide. Its mobility in room temperature air (Z_s = 0.599 cm^2V/s)[27] was determined by comparison with the analogous ion $(C_7H_{15})_4N^+$, also electrosprayed from its bromide solution in ethanol.[28] This mobility of C_{18} agrees with that recently reported in N_2 at 300 K,[29] with slight differences compatible with the present different temperature and drift gas. The sheath gas used by the DMA was room air at its ambient humidity, with a minimal contribution of CO_2 from the much smaller flow of sample gas. The detector used for the DMA-selected ions was not the sensitive CNC used in GEMMA. Instead we relied an operational amplifier electrically connected to a HEPA filter encased in a Faraday cage, where the current of mobility-selected ions in the air flow exiting the DMA at a flow rate of 2–3 L/min was captured and measured. This electrical detector is sensitive enough in our system to give good signal/noise at ~1 μM protein concentration. Experiments without charge-reduction were performed by unscrewing the Cajon fitting holding the Ni-63 from the ES chamber and replacing it with an almost identical fitting not containing the radioactive element.

Ovalbumin (chicken egg) and immunoglobulin IgG (rabbit), both from Sigma, were used mostly without any desalting or other purification. In a few final measurements, ovalbumin was desalted six successive times by centrifugal ultrafiltration of 0.5 mL of a 75 μM solution in deionized water (PALL Corporation, cutoff mass of 10 kDa). Ammonium acetate and a solution 1 M of triethylammonium formate (TEAF) in water were from Fluka. $(C_{18}H_{37})_4N-Br$ and $(C_7H_{15})_4N-Br$ were from Sigma-Aldrich and Alfa Aesar, respectively.

Electrospraying fused silica capillary emitters 365 μm in outer diameter were either purchased from New Objective (30 μm tip pulled from an original inner diameter of 70 μm) or home-pulled under a flame from a commercial silica capillary (Polymicro). The home-pulled tips spanned diameters from ~15 down to a few micrometers. The larger tips were polished on a flat rotating alumina surface while rotating the capillary by hand about its axis.

RESULTS

Figure 2 compares two mobility spectra without charge-reduction, while electrospraying from an aqueous buffer 100 mM in TEAF. One spectrum is for the plain buffer (blank), while the other includes 3 μM Ovalbumin. Ions classified in the inner electrode at high negative voltages are dragged by the sample gas to ground potential against the field inside a semiconducting tube. The sample gas flow rate through the ES chamber into the DMA inlet is 1 L/min. The amplifier response shown in the figures is in volt, with a noise level of a few mV. The blank shows a diversity of reasonably resolved high mobility peaks extending down to −120 V, with a maximum signal of 4.2 V. This is followed by a broad shoulder extending to −230 V, with a maximum intensity of some 70 mV. A similar shoulder is also present in the protein sample and is due in both cases to solid residues from dried ES drops not containing protein ions. This involatile matter is evidently also

DOI: 10.1021/ac504445n
Anal. Chem. XXXX, XXX, XXX−XXX

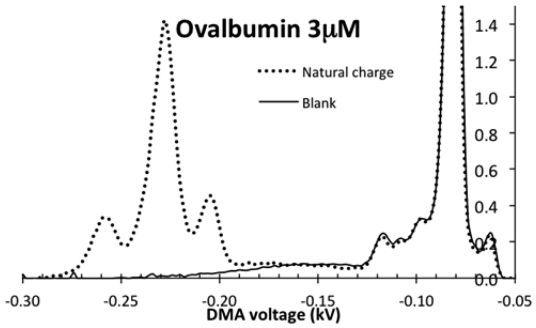

Figure 2. Mobility spectra without charge-reduction. Continuous line: blank buffer (100 mM TEAF in H_2O). Dotted line: 3 μM ovalbumin in charge states z = 7, 8, 9. The shoulder between −230 and −120 V is associated with volatile impurity residues from dried drops.

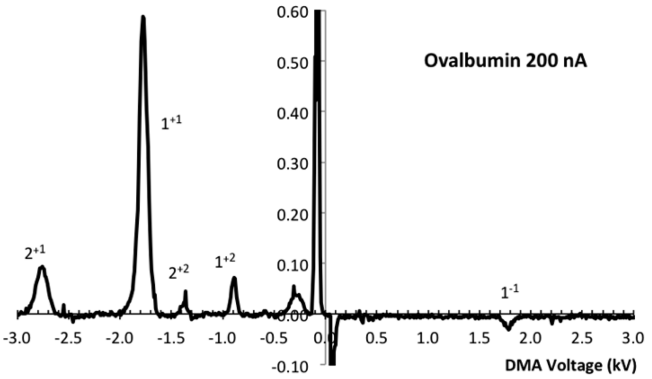

Figure 3. Bipolar mobility spectrum displaying a small charge-inverted peak 1^{-1}. Gridless configuration with nanospray capillary; $L \sim 0.75$ mm.

present in drops containing proteins, and its adduction to the protein ion is responsible for a fraction of the extra peak broadening previously discussed. These adducts are often removed in the intermediate pressure entry region to mass spectrometers, but this *declustering* process is harder to implement at atmospheric pressure. A high-quality electrospray and a singularly clean sample are therefore most important to achieve narrow peaks. The three multiply charged protein peaks seen in Figure 2 give a total signal of about 2.2 V, comparable to the total buffer ion signal of about 5 V, and close to 3 orders of magnitude above the electrometer noise. Large space charge losses through the sampling process dilute selectively high mobility species, explaining part of the relative abundance of protein/buffer observed.

Gridless Configuration with Nanospray Tips. When the partition between the two chambers is the original 5 mm thin plate orifice (gridless), the capillary tip can freely cross from one chamber to the other. As further illustrated in the Supporting Information (Figure S-1), a home-pulled and sharpened capillary with an unusually small outer tip diameter (~1 μm) produced a stable ES current even when the emitter was within the charge-reduction chamber. On moving axially, the tip of the emitting capillary, from a maximum distance $L \sim$ 6 mm toward the thin plate orifice partition, the protein peak increased in height, with no clear sign of peak broadening. However, with the ~~needle~~ right at the partition but before reaching it and slightly past the partition, the peak height decreased moderately (~30%), as the peak width almost tripled. It is unclear if this drastic broadening is due to deterioration of the spray quality (due to the conducting gas surrounding the Taylor cone) or to partial suppression of secondary atomization (due to early neutralization of the drops). Either way, it is clear that the details of the coupling between the ES and the charge reduction chamber may have drastic effects on resolution.

Charge Inversion. Figure 3 shows a bipolar mobility spectrum meant to capture the small fraction of charge-inverted ions resulting from negative charging of fully neutralized proteins. The data are acquired with the nanospray tip in gridless configuration. The notation n^{+z} represents an aggregate of n protein molecules carrying a net balance of z positive elementary charges. There is a clear 1^{-1} peak, whose height is about 20 times less tall than the 1^{+1} peak. One reason for this low signal is the substantially smaller cross section for ion−neutral collisions than for collisions between oppositely charged ions. Since the residence time of the system is designed for the later collision types, there is insufficient time for charge inversion. It is however possible to enhance substantially this negative signal. For instance, McLuckey and colleagues,[30] have not only illustrated the mass spectrometric advantages of charge permutation but have also achieved it with high cross sections via multiply charged counterions. This is not possible with our source, but the inverted signal would be considerably enhanced if the residence time were appropriately tuned or if our electrical detector were exchanged for a CNC. One advantage of charge inversion is that a near ~~equilibrium~~ charge distribution may be achieved at long enough times, at which the probability p_2 of double charging is small compared with the probability p_1 of single charging, the (size-dependent) ratio p_2/p_1 is approximately predictable, and p_1 is scarcely dependent on residence time.[31] The resulting ion concentrations in inverted polarity are accordingly far less critically dependent on initial charge and size than when tuning the residence time to maximize the output of z = 1 ions of a certain initial charge state.

The data discussed so far are of interest to illustrate what can be achieved with nanospray capillaries that minimize the destabilizing effects of the charge-reducing ion cloud on the emitter. However, this interaction is very sensitive to tip geometry, leading to hard to reproduce results when the sharpening technique is not very well controlled. For instance, using commercial Picotip capillaries from New Objective pulled into a 30 μm tip o.d. from an initial 100 μm capillary i.d., it is rather hard to stabilize the Taylor cone even when the emitting tip is 3 mm away from the thin plate orifice. It is interesting that the GEMMA approach is apparently not subject to these problems yet uses typically a distance L of 3 mm and relies on tip diameters in the range of 30 μm or more, producing clearly visible Taylor cones. A possible cause for this difference is the much larger volume in the GEMMA charge-reduction chamber, probably limiting the magnitude of the negative ion current that may be drawn into the electrospray region. As long as this current is small enough to be fully consumed in the spray region, without reaching the continuous jet at the tip of the Taylor cone, it cannot affect the stability of the meniscus.

Gridded Configuration. In view of the spray stability difficulties encountered and in order to maintain our compact charge-reduction chamber geometry, we have sought to reduce the penetration of the tip's electric field into the bipolar ion cloud region by reducing with a washer the aperture of the sharp edge orifice. This greatly increase ES stability but diminishes the efficiency of charge-reduction because the flow

DOI: 10.1021/ac504445n
Anal. Chem. XXXX, XXX, XXX−XXX

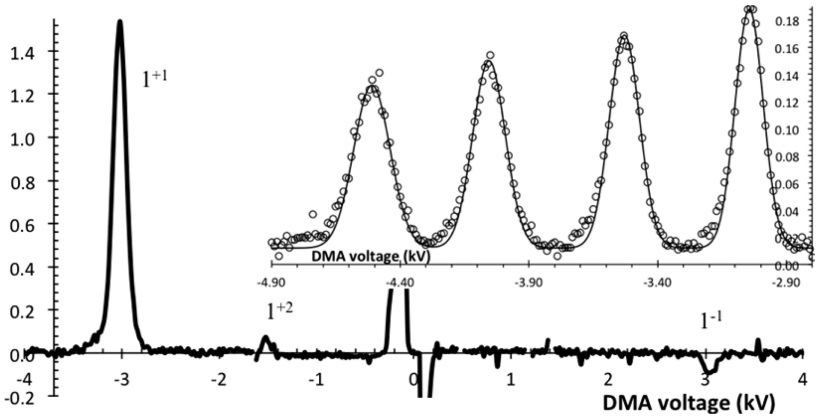

Figure 4. Mobility spectra of ovalbumin for the gridded geometry. Thick line: Bipolar spectrum, showing a dominant 1^{+1} ion, with 5% and 6% relative contributions from the $z = +2$ and the $z = -1$ ions, respectively (sample flow rate, 2.5 L/min; two Ni-63 rings in series; 2 μM ovalbumin in 100 mM aqueous ammonium acetate). Inset: four peak shapes for ovalbumin's 1^{+1} ion at four flow rates of drift gas increasing from right to left, demonstrating $fwhm_{min} < 3; 7\%$ for peaks above 4 kV (Table 1).

of gas going through a smaller opening forms a narrower and faster jet, reducing the time and volume of contact with the bipolar ions. A better partition avoiding this jetting is a metallic grid. For instance, with a square mesh (0.01 in. wire diameter, 30 wires/in.) placed immediately downstream the thin plate orifice partition, the spray is as stable with the radioactive Ni-63 piece in place as without it, even when the capillary tip is brought very close to the partition. The following tests including this gridded geometry have used ovalbumin solutions in 50−100 mM buffers of aqueous ammonium acetate. This salt produces an initial charge state $z_{in} \sim 14$ considerably greater than TEAF, enabling a more rigorous challenge of the charge-reducing capacity of the device.

Figure 4 illustrates both the efficient charge reduction for ovalbumin ions as well as the relatively narrow peaks achievable in the gridded geometry. The sample flow rate is slightly more than twice that in Figure 3, while the power of the radioactive source has been doubled (20 mCi). The charge reduction power is accordingly similar in both figures, as seen in the comparable intensity ratios $1^{-1}/1^{+1}$. In spite of the higher initial charge state achieved in ammonium acetate solutions, the level of neutralization is much enhanced by the grid, as evidenced by the ratio of abundances $1^{+1}/1^{+2}$ (~20 here versus ~9 in Figure 3). This improvement is not surprising because anions penetrating into the gridless ES chamber would be wasted in reactions with the drops, while a later interaction following complete drop evaporation would preferentially direct those anions into the most highly charged remaining cations (the proteins). Comparison of peak heights taken at the same sample flow rate in gridless (Figure 3) versus gridded spectra (Figure S-2 in the Supporting Information) show a ~1/2 loss of signal in the grid, readily understood given its ~50% transparency. In our situation with no externally imposed electric field following the grid, one might have feared much larger losses due to the protein ions being directed to the mesh by the electric field upstream the grid. The lack of this extra loss indicates that the ES ions self-propel themselves through the screen and downstream from it by their strong space charge field. This implies that the relatively good transmission efficiency of ions through the present grid would be further improved in a more transparent grid. This would not necessarily imply an undesirable increased anion penetration into the ES region, since this penetration is governed by the size of the opening, which may be controlled independently of transparency by selecting a smaller wire.

On the Width of Charge-Reduced Peaks. The thick line data of Figure 4 correspond to fwhm ~4.9% for the 1^{+1} ion. In other measurements and in Figure 3 we have seen considerably wider peaks (7% in Figure S-1 in the Supporting Information), depending on the cleanness of the solution, the quality of the spray, and the flow rates through the DMA. With a freshly made solution of 2.5 μM ovalbumin in 50 mM aqueous ammonium acetate, we have achieved fwhm as small as 0.043−0.045, with an observable dependence on DMA parameters. With a moderate desalting effort (via centrifugal ultrafiltration) this width was reduced only slightly down to fwhm = 0.042, suggesting that perhaps some of the impurity ions attached to the protein are internal rather than on the surface. Reference 14 suggests that this possible mode of contamination might be reduced in the case of denatured proteins. We have accordingly briefly investigated a 30 μM ovalbumin solution in 50 mM ammonium acetate including 5% formic acid (inset to Figure 4). Peaks centered at increasing voltages result from increasing flow rates of drift gas in the DMA, with corresponding fwhm values collected in Table 1. The acidified solution delivers somewhat narrower peaks than the ammonium acetate buffer, with fwhm as small as 0.037. The dependence of this width on DMA setting shows that the instrument has some limiting effect on resolution, suggesting that the intrinsic width of the protein peak may be closer to 3% in desalted acidified solutions.

Table 1. Peak Width in Gridded Configuration for the Singly Charged Ovalbumin Monomer of Figure 4 (Inset) at Varying DMA Drift Gas Velocities

peak voltage (kV)	3.04	3.53	4.06	4.51
fwhm (%)	4.22	3.92	3.67	3.69

Acidification of the solution results in modestly narrower peaks as well as mobilities slightly larger (~3−4%) than in ammonium acetate. This reduction in cross section is comparable to the variations observed upon increasing the quality of the spray and may be due to a decrease in adduction rather than to a real compaction of the structure.

Figure 5 shows the mobility spectrum of a concentrated ovalbumin solution producing protein aggregates. It is taken under similar spraying conditions as the inset to Figure 4,

DOI: 10.1021/ac504445n
Anal. Chem. XXXX, XXX, XXX−XXX

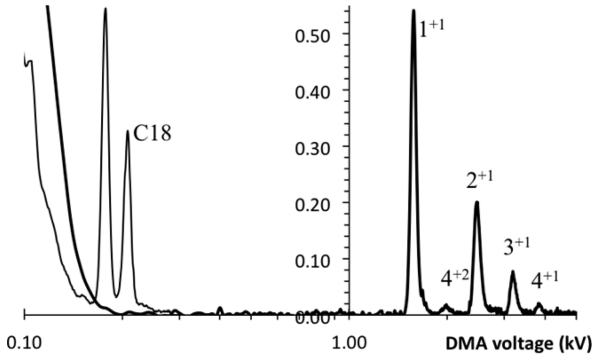

Figure 5. Mobility spectrum of 30 μM ovalbumin including 50 mM ammonium acetate and 5% formic acid (thick line), showing clear peaks from the monomer to the tetramer. The two peaks on the left are from the much more mobile $(C_{18}H_{37})_4N^+$ calibration standard.

though with a lower sheath gas flow rate and an increased sample flow rate of 1.5 L/min of dry air (rather than CO_2) through the ES chamber (only one Ni-63 source). These different operating conditions of the DMA increase substantially the signal and widen the mobility range (as needed to capture the tetramer peak 4^{+1}). However, they limit the resolution (Table 2) and the charge-reduction power of the device (i.e., survival of the doubly charged tetramer at about 2 kV). The figure includes also the calibrant ion $(C_{18}H_{37})_4N^+$, enabling determination of the room temperature mobilities of ovalbumin and its aggregates. Their magnitudes are compared in Table 2 to those of ~~Meisser~~ et al.,[14] showing almost an identical value for denatured 1^{+1}. Surprising, their denatured 2^{+1} is substantially more mobile than ours, a property shared also by half the mobility of their denatured 2^{+2}. This is unusual, as the compactness parameter $n^{2/3}Z$ tends to be relatively independent of n for proteins and largest for the monomer.[33] This expected trend is approximately followed by our data up to the tetramer. However, in the denatured data of ~~Meisser~~ et al.,[14] $n^{2/3}Z$ is considerably larger for the dimer (0.0733 $cm^2\ V^{-1}\ s^{-1}$) than for the monomer (0.0670 $cm^2\ V^{-1}\ s^{-1}$). The effective dimer densities were not calculated in ref 14 but would be singularly large, about 15% above those reported for ovalbumin. Table 2 includes also published mobilities for higher charge states, with Z/z values comparable to ours (including the dimer), though slightly lower (as usual) due to the higher charge state.[34,35]

Knowing the expected width of protein peaks enables an estimate of the number of individual biomolecules that could be distinguished in a complex mixture. We focus on proteins ranging in mass from 0.1 to 4 MDa, whose singly charged ions would be much harder to analyze with conventional MS detectors. Their surface areas (assuming them to be spheres) and therefore their electrical mobilities with $z = 1$ would span approximately a range $40^{2/3}$. The number N of different proteins that could be differentiated if fwhm were 3% can be estimated as $N = \log(40^{2/3})/\log(1.03) = 83$.

Extrapolations to Larger Proteins. Because the time theoretically required for reducing the initial charge state z_{in} of a globular ion to unity scales with its mass m as $\ln(z_{in}) \sim \ln(m)/2$, a slow deterioration of the charge reduction efficiency (in the form of an increased survival of $z = 2$ ions) should be expected at increasing masses. Besides the ovalbumin multimer measurements of Figure 5, we have done a limited exploration of the charge-reduction ability of our device with electrosprays of the larger protein IgG (~150 kDa) as well as aggregates of IgG (up to the trimer; Figure S-3 in the Supporting Information). At a sample flow rate of 1.5 L/min, the observed level of charge reduction is insufficient at 300 kDa but becomes adequate at half that flow. In a few exploratory experiments introducing two 10 mCi Ni-63 sources into the charge-reduction chamber, we have confirmed that the sample flow rate can be increased approximately 2-fold while preserving the same $z = 1$ to $z = 2$ abundance ratio. Accordingly, achieving proper charge reduction with samples of several MDa will probably require the wider charge-reduction chambers having previously shown an ability to handle much larger virus particles.[11,23]

CONCLUSIONS

We have studied the possibility to achieve improved resolving powers in the mobility analysis of large charge-reduced ions using a differential mobility analyzer of relatively high resolution and a charge-reduction method exploiting the full atomizing power of high conductivity electrosprays (nanospray). Spray quality and sample cleanness have a large impact on peak broadening, but for desalted and acidified samples, singly charged protein peaks with fwhm as small as 3.7% are found. This lower bound is partly limited by DMA resolution and lack of thorough removal of involatile impurities, suggesting that intrinsic charge-reduced protein peak widths may be closer to 3%. Assuming that this fwhm may be extrapolated to MDa ions, the method would permit distinguishing 83 different proteins with evenly spaced masses spanning the region from 10^5 Da to to 4 MDa. The established GEMMA approach of neutralizing the drops before they dry has quantification advantages, though at a high cost in terms of resolution.

ASSOCIATED CONTENT

Supporting Information

Performance of the gridless configuration with a nanospray tip inside and outside the charge-reduction chamber, additional information on the operation of the gridded chamber, and performance of the gridded charge-reduction chamber with IgG

Table 2. Peak Voltages, Widths, and Corresponding Electrical Mobilities in Room Temperature Air for the Singly Charged Ions of Ovalbumin and Its Aggregates with $n \leq 4$

	V (kV)	fwhm (%)	Z ($cm^2\ V^{-1}\ s^{-1}$)	$n^{2/3}Z$ ($cm^2\ V^{-1}\ s^{-1}$)	Z^{14} ($cm^2\ V^{-1}\ s^{-1}$)	$n^{2/3}Z^{14}$ ($cm^2\ V^{-1}\ s^{-1}$)	$n^{2/3}(Z/z)^{32}$ ($cm^2\ V^{-1}\ s^{-1}$)
C_{18}	0.177	5.61	0.5990	0.5990			
$n = 1$	1.579	4.50	0.0671	0.0671	0.0602[a]/0.0670[b]	0.0602[a]/0.0670[b]	0.0638[c]
$n = 2$	2.475	5.16	0.0428	0.0679	0.0462[b]	0.0733[b]	0.0418[d]
$n = 3$	3.199	4.75	0.0331	0.0689			0.0319[e]
$n = 4$	3.840	3.96	0.0276	0.0695			

[a]Native. [b]Denatured. [c]$z = 8$. [d]$z = 15$. [e]$z = 17$.

DOI: 10.1021/ac504445n
Anal. Chem. XXXX, XXX, XXX−XXX

and its aggregates up to the trimer. This material is available free of charge via the Internet at http://pubs.acs.org.

AUTHOR INFORMATION

Corresponding Author

*E-mail: juan.delamora@yale.edu.

Notes

The authors declare the following competing financial interest(s): Following Yale rules, the author declares his personal interest in the companies SEADM and Nano-Engineering Corporation, commercializing the DMA used here.

ACKNOWLEDGMENTS

I thank Michel Attoui (U. Paris), Gonzalo Fernández de la Mora (SEADM), and Jerome J. Schmitt III (NanoEngineering Corporation, NEC) for stimulating my interest in ionization and charge-reduction in bipolar ion sources. Also thanks to M. Attoui, Juan Fernández Garcia, and Aaron Madden for many contributions to the DMA facility and to Shumin Bian and Ionel Hau for advice on radioactive sources. Partial support was received from SEADM, NanoEngineering Corporation, and DARPA Grant W31P4Q13C0073 (Connecticut Analytical Corporation subcontract). I am particularly grateful to Dr. Stan Kaufmann for noting the interest of ambient pressure charge inversion and for many GEMMA-related discussions over the years.

REFERENCES

(1) Fenn, J. B.; Mann, M.; Meng, C. K.; Wong, S. F.; Whitehouse, C. M. *Science* **1989**, *246*, 64−71.
(2) Wong, S. F.; Meng, C. K.; Fenn, J. B. *J. Phys. Chem.* **1988**, *92*, 546−550.
(3) Reid, G. E.; Wells, J. M.; Badman, E. R.; McLuckey, S. A. *Int. J. Mass Spectrom.* **2003**, *222*, 243−258.
(4) Scalf, M.; Westphall, M. S.; Krause, J.; Kaufman, S. L.; Smith, L. M. *Science* **1999**, *283*, 194−197.
(5) Kaufman, S. L.; Skogen, J. W.; Dorman, F. D.; Zarrin, F.; Lewis, K. C. *Anal. Chem.* **1996**, *68*, 1895−1904.
(6) Fernández de la Mora, J.; Kozlowski, J. *J. Aerosol Sci.* **2013**, No. 57, 45−53.
(7) Kaufman, S. L. *J. Aerosol Sci.* **1998**, No. 29, 537−552.
(8) Oberreit, D. R.; McMurry, P. H.; Hogan, C. J., Jr. *Aerosol Sci. Technol.* **2014**, *48* (1), 108−118.
(9) Wang, J.; McNeill, V. F.; Collins, D. R.; Flagan, R. C. *Aerosol Sci. Technol.* **2002**, *36* (6), 678−689.
(10) Knutson, E. O.; Whitby, K. T. *J. Aerosol Sci.* **1975**, *6*, 443−451.
(11) Guha, S.; Li, M.; Michael, J.; Tarlov; Zachariah, M. R. *Trends Biotechnol.* **2012**, *30*, 291−300.
(12) Kaddis, C. S.; Lomeli, S. H.; Yin, S.; Berhane, B.; Apostol, M. I.; Kickhoefer, V. A.; Rome, L. H.; Loo, J. A. *J. Am. Soc. Mass Spectrom.* **2007**, *18*, 1206−1216.
(13) Bacher, G.; Szymanski, W. W.; Kaufman, S. L.; Zollner, P.; Blaas, D.; Allmaier, G. *J. Mass Spectrom.* **2001**, *36*, 1038−1052.
(14) Maisser, A.; Premnath, V.; Ghosh, A.; Nguyen, T. A.; Attoui, M.; Hogan, C. J. *Phys. Chem. Chem. Phys.* **2011**, *13*, 21630−21641.
(15) Fernández de la Mora, J.; Ude, S.; Thomson, B. A. *Biotechnol. J.* **2006**, *1*, 988−997.
(16) Martínez-Lozano, P.; Fernández de la Mora, J. *J. Aerosol Sci.* **2006**, *37*, 500−512.
(17) Ku, B. K.; Fernandez de la Mora, J.; Saucy, D. A.; Alexander, J. N. *Anal. Chem.* **2004**, *76*, 814−822.
(18) Saucy, D. A.; Ude, S.; Lenggoro, I. W.; Fernandez de la Mora, J. *Anal. Chem.* **2004**, *76*, 1045−1053.
(19) Laschober, C.; Kaddis, C. S.; Reischl, G. P.; Loo, J. A.; Allmaier, G.; Szymanski, W. W. *J. Exp. Nanosci.* **2007**, *2* (4), 291−301.
(20) Konermann, L.; Ahadi, E.; Rodriguez, A. D.; Vahidi, S. *Anal. Chem.* **2013**, *85*, 2−9.
(21) Consta, S.; Malevanets, A. *Phys. Rev. Lett.* **2012**, *109*, 148301.
(22) Fernandez de la Mora, J. *Anal. Chim. Acta* **2000**, *406*, 93−104.
(23) You, R.; Li, M.; Guha, S.; Mulholland, G. W.; Zachariah, M. R. *Anal. Chem.* **2014**, *86*, 6836−6842.
(24) de Juan, L.; Fernández de la Mora, J. *J. Colloid Interface Sci.* **1997**, *186*, 280−293.
(25) Kaufman, S. L., Zarrin, F. Dorman, F., U.S. Patent No. 5,247,842, 1993.
(26) Fernandez de la Mora, J. *Annu. Rev. Fluid Mechanics* **2007**, *39*, 217−243.
(27) Fernández de la Mora, J. *Aerosol Sci. Technol.* **2015**, *49* (1), 57−61.
(28) Ude, S.; Fernández de la Mora, J. *J. Aerosol Sci.* **2005**, *36*, 1224−1237.
(29) May, J. C.; Goodwin, C. R.; Lareau, N. M.; Leaptrot, K. L.; Morris, C. B.; Kurulugama, R. T.; Mordehai, A.; Klein, C.; Barry, W.; Darland, E.; Overney, G.; Imatani, K.; Stafford, G. C.; Fjeldsted, J. C.; McLean, J. A. *Anal. Chem.* **2014**, *86*, 2107−2116.
(30) He, M.; McLuckey, S. A. *J. Mass Spectrom.* **2004**, *39* (11), 1231−1259.
(31) Friedlander, S. K. *Smoke, Dust, and Haze: Fundamentals of Aerosol Dynamics*; Oxford University Press: New York, 2000.
(32) Hogan, C. J.; Fernandez de la Mora, J. *J. Am. Soc. Mass Spectrom.* **2011**, *22*, 158−172.
(33) Fernandez de la Mora, J.; Borrajo-Pelaez, R.; Zurita-Gotor, M. *J. Phys. Chem. B* **2012**, *116*, 9882−9898.
(34) Hogan, C.; Ruotolo, B.; Robinson, C.; Fernandez de la Mora, J. *J. Phys. Chem. B* **2011**, *115* (13), 3614−3621.
(35) Fernandez de la Mora, J.; Borrajo-Pelaez, R.; Zurita-Gotor, M. *J. Phys. Chem. B* **2012**, *116*, 9882−9898.

DOI: 10.1021/ac504445n
Anal. Chem. XXXX, XXX, XXX−XXX